EasyChair Preprint

№ 2739

A Comprehensive Study on Electronic Structure and Optical Properties of the A3(SF)2(a=Hg, Pb)

Salman Khan, Sikander Azam, Muhammad Irfan,
Muhammad Farooq Nasir and Amin Ur Rahman

February 21, 2020

A comprehensive study on electronic structure and optical properties of the $A_3(SF)_2$(A=Hg, Pb)

Salman Khan[1], Sikander Azam[2], Muhammad Irfan[1], Muhammad Farooq Nasir[2], Amin Ur Rahman[2]

1Department of Physics, The University of Lahore, Sargodha campus, 40100 Sargodha, Pakistan

[2]Department of Physics Riphah International University Sector I-14 Islamabad, Pakistan.

The Women University Multan, 66000, Multan.

Abstract

Here we reported the electronic and optical properties for cubic phase $A_3(SF)_2$ where (A=Hg, Pb) under the precise density functional theory (DFT) by using the accurate Tran–Blaha modified Becke–Johnson exchange potential approximation (TB-mBJ) as an exchange-correlation functional. In this work we for the first time investigated all the optical and electronic properties of $A_3(SF)_2$. The real and imaginary dielectric functions were explored along with optical absorption coefficient, reflectivity, energy loss function, refractive index and extinction coefficient. We demonstrated the direct and indirect band gap nature of these materials. Our investigation explained that the two materials sustain their positive value of refractive index and thus are non negative index metamaterials.

Keywords: electronic band structure, optical properties, DFT, TB-mBJ, wien2k.

1. Introduction

Now a days, researchers are struggling to discover materials having potential uses like hydrogen sensors, data storage devices such as random access memory, fuel cells, high intensity violet and blue light emissions, optical wave-guides, high temperature oxygen sensors and capacitors in different functional devices [1-2]. Among these Ternary compounds belonging to group II-VI-VII has also been attracted a growing concentration because of their potentials applications in the integrated optics and photovoltaic [3]. These ternary type complexes are also promising materials for various optoelectronic applications [4-6]. We investigated for the first time $Hg_3(SF)_2$ and $Pb_3(SF)_2$ which are also promising members of this group. Due to the toxic nature of mercury, only a small number of reports relating to the synthesis of mercury based ternary compounds are exposed. In these reports, researchers prepared Hg (S, Se, Te) nano particles at room temperature and influence of different parameters like capping agent, power of irradiation, temperature and reducing agent type on morphology of their products were studied [7-9]. It is observed that the liquid mercury initially changed to a golden crystalline mass and the reaction

of liquid mercury with a solution of AsF forms the compounds $Hg_3(AsF_6)$ and Hg(AsF) these results showed that in this compound in fact undergoes a remark-able transformation to give a unique metallic bonded infinite polymeric cations [10]. Similarly the mixed valent mercury compounds $Hg_3(HAsO_4)_2$ and $Hg_6As_2O_{10}$ were obtained due to the reaction of $Hg_3(AsO_4)_4$ with arsenic acid, this Intensity data of $Hg_3(HAsO_4)_2$ were recorded at –143 ◦C on a Siemens SMART CCD diffractometer using ω scans with 0.3˚ rotation width in addition the intensity data of $Hg_6As_2O_{10}$ was also recorded at room temperature [11]. The corresponding crystal structures were solved by implementing direct methods and refined by using the SHELXTL program package [12]. In terms of the diffuse reflectance and microscopic infrared spectra the optical properties of a new mixed-framework mercury selenide diselenite, $(Hg_3Se_2)(Se_2O_5)$ were studied. The electronic band structure and the density of states (DOS) were calculated by the DFT method which indicates that the compound was a semiconductor, and its optical absorption is mainly attributed due to charge transitions from the O-2p and Se(II) 4p states to the Se(IV) 4p and Hg-6 s-states [13]. Various complex modulations and structural disorder was exhibited by the crystals of the $Hg_3Se_2Bi_2Cl_8$, which show complication in its structural refinement, in addition the compound melt incongruently and show band gaps of 3.26 eV, which were in a perfect agreement with the band-structure from density functional theory calculations [14].

In the present work the electronic and optical properties of Mercury and silver based difluoride disulfide are theoretically studied under the frame work of density functional theory (DFT) using (TB-mBJ) approximations in the FP-LAPW method. To the best of our knowledge there is a lack of experimental and theoretical data on the structural, electronic and optical properties of cubic $Hg_3(SF)_2$ and $Pb_3(SF)_2$.

2. Computational and calculation details

Basic computational calculations of our analysis are performed by using the full potential linearzed augmented plane wave (FP-LAPW) as based on the well known density functional theory (DFT) which is implemented in Wien2k package. In addition, Kohn-Sham equations are calculated by applying full potential-linearized augmented plane wave (FP-LAPW) using self consistent method [15-19]. In order to divide the space into two regions, the Slater's theory of Muffin-Tin radii has been used close to the atoms in the FP-LAPW method, beside this all the interesting parameters are expanded in terms of spherical harmonics and as the expansion of the plane waves along with wave vector which have cut-off value of K_{MAX} in the given interstitial region. The first kind of expansion is demonstrated within an eminent muffin-tin sphere of radius RMT which is around every nucleus. The choice of spherical radii predicts the rate of convergence of these analyzed expansions, but this affects the rate of the calculations. We choose R_{MT} x K_{MAX} = 7 (Rmt is known as the smallest of all MT sphere radius and Kmax is the maximum value of the wave vector K), as convergence parameters for the matrix element which shows the number of fundamental functions, in addition to which K_{MAX} is associated with plane wave cutoff in momentum space (k-space) and the R_{MT} represent smallest radius of Muffin-Tin cube among all the atomic spherical radii. For the calculation the energy separation is considered

to be at -6 Ry. In order to calculate the exchange correlation potential we used the modified Becke-Johnson exchange potential, this approach provides accurate band gap and optical properties results which are in good agreement with the experimental data [20]. We selected the maximum value of l as l_{max} =10 for the wave function expansion within the atomic spheres while outside the muffin-tin spheres, fourier series is used for the expansion of charge density. In order to achieve self-consistency the reciprocal space integration under different pressure values in the Brillouin zone, we choose 500 k-points in grid of 10 ×10 ×10 meshes which is equal to 1000-k points in the complete Brillouin zone scheme has been employed. The corresponding dielectric function $\varepsilon(\omega)=\varepsilon_1(\omega)+i\varepsilon_2(\omega)$ which consist of real and imaginary dielectric parameters are used to study the optical characteristics of the two materials. Ehrenreich and Cohen give brief description concerning the real and imaginary parts of dielectric function which is formulated and given by the following equations [21,22].

$$\varepsilon(\omega) = \frac{e^2\, h'}{\pi m^2 \omega^2} \sum_{v,c} \int_{BZ} |M_{cv}(k)|^2 \delta[\omega_{cv}(k) - \omega] d^3k$$

In the above equation the volume integral is limited only to first Brillouin zone and corresponding dipole matrix element $M_{cv}(k)=u_{ck}/e\Delta/u_{vk}$ gives the details about direct transition between valence band and conduction band states. The relation $\omega_{cv}(k) = E_{ck} - E_{vk}$ gives the account of the excitation energy used during the transition between conduction and valence band states, here "e" represents polarization vector due to the electric field and "u_{ck}" give details about the periodic portion of the Bloch wave function in conduction band which is totally associated with wave vector k. The unit cell structure for both the two compounds is demonstrated in Figure 3(a) and 3(b). It shows a cubic symmetry having space group, Hermann Mauguin $I2_13$ [199] and point group of 199.

3. Results and discussion

3.1 Band structure and density of states

In the development of magneto-optic, magneto electronic and optoelectronic the knowledge about the band gap and electronic band structure is too much necessary. The electronic band structure plays an important role in the study of electronic properties of material. The origin of electronic band structure is directly related to the density of state (DOS). The study of band structure allows us to evaluate the spectral distribution of the absorption, charge density distribution, their mobility etc [23]. Our evaluated optical characteristics may serve as a base for the further optimization of the electronic properties in the desired direction. The calculated band structure dispersion in k-space along with high symmetry directions in the BZ, the total and partial density of states are presented in Fig.1 and Fig.2.The energy scale is in eV, was arbitrarily set to be at the top of valance band. The electronic band structure of $A_3(SF)_2$ which is shown in Fig.1 demonstrate that the material is found to be an indirect band gap material. The energy band

gap direct point Γ-Γ for $Pb_3(SF)_2$ is found to be 0.53 eV and for $Hg_3(SF)_2$ is found to be 2.5 eV. The indirect band gap of 2.5 eV at the Γ point for $Hg_3(SF)_2$ reveals that the top of the valance band is very flat, which definitely suggest a very large effective hole mass, and therefore we may conclude that the dominating charges carriers in $Hg_3(SF)_2$ are electrons. The angular momentum character of the various structures is identified by the help TDOS and PDOS. In order to understand the contribution of each orbital in these atoms we have plotted the angular momentum decomposition of partial density of states (PDOS). Fig. 2(a) and 2(b) shows total (TDOS) and partial density of states (PDOS) of $Hg_3(SF)_2$ and $Pb_3(SF)_2$, the lowest structure in case $Hg_3(SF)_2$ extended from -2.0 eV to 10.0 eV originates mainly from Hg-f, S-s and F-p states with small admixture of S-p, F-s states which shows that these orbital are spatially delocalized. The partial densities of states (PDOS) indicates the hybridization between the electronic states of the elements (A= Hg,Pb), S and F. subsequently the next energy fragment is from -2.0 eV to the Fermi level (EF) which is at 0 eV and originates from more localized Hg-d states with a small contribution from S-p, F-p states. The conduction band minima (CBM) have contributions principally from S-p states where the valence band maxima (VBM) are dominated by the Hg-f states. Similarly as incase of $Pb_3(SF)_2$ the lowest structure extended from -2.0 eV to - 0 eV originates mainly from Pb-p, S-p and F-p states with small admixture of S-s, F-s states. Similarly the next energy fragment for $Pb_3(SF)_2$ is from -2.0 eV to the Fermi level originates from the most localized Pb-d states with a minute contribution from S-p, F-p states. The fig. 3b shows that the maximum contribution around the Fermi level is of Pb-f states. The first peak in the conduction band at 0.9 eV is mainly because of Pb-p state and maximum peak at 3.5 eV is due to unoccupied f states of Pb.

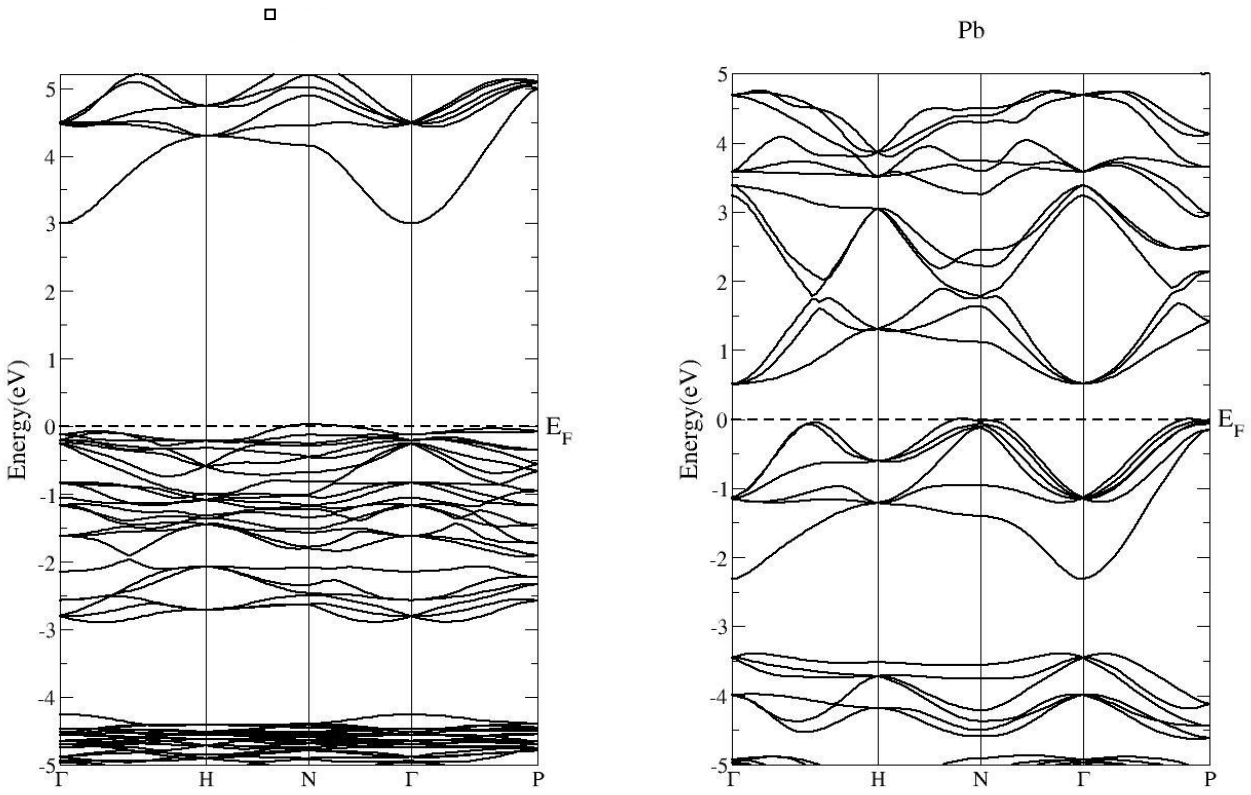

Fig. 1(a) and 1(b): Calculated band gape structure for both the compounds $A_3(SF)_2$ A= (Hg, Pb)

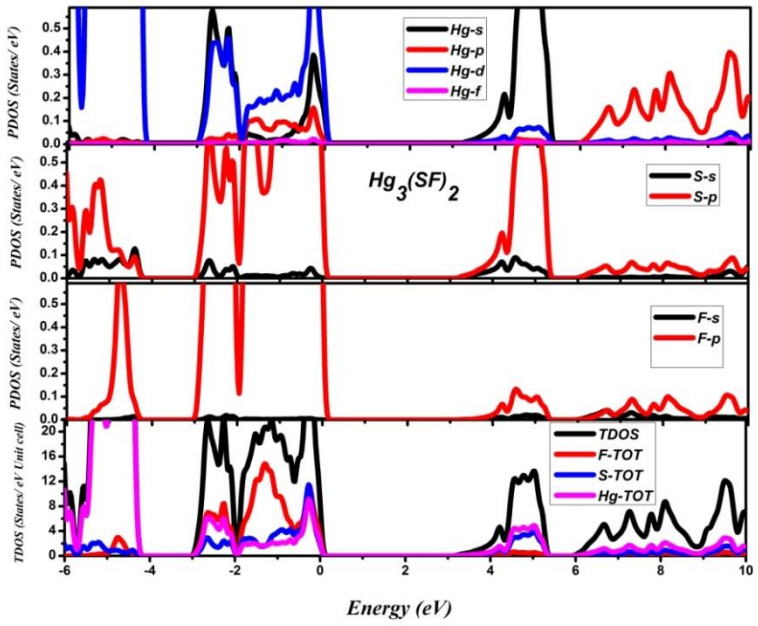

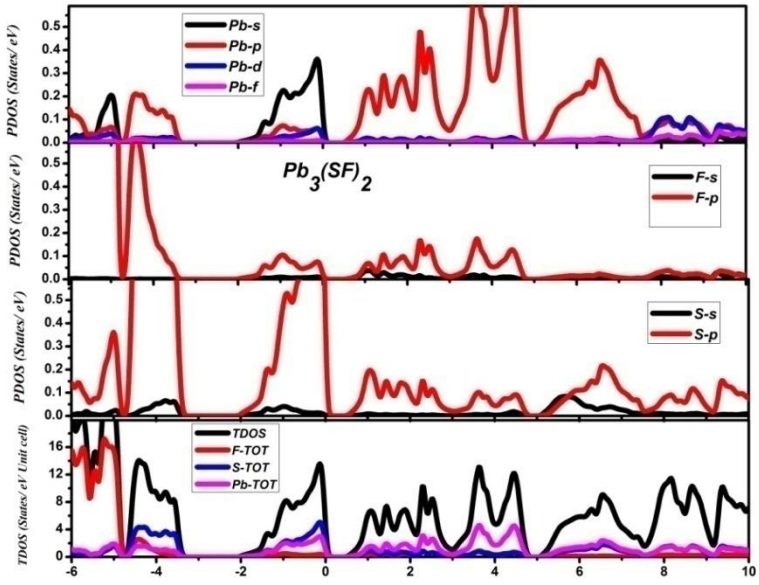

Fig. 2(a) and 2(b): Calculated TDOS and PDOS of $A_3(SF)_2$ A= (Hg, Pb)

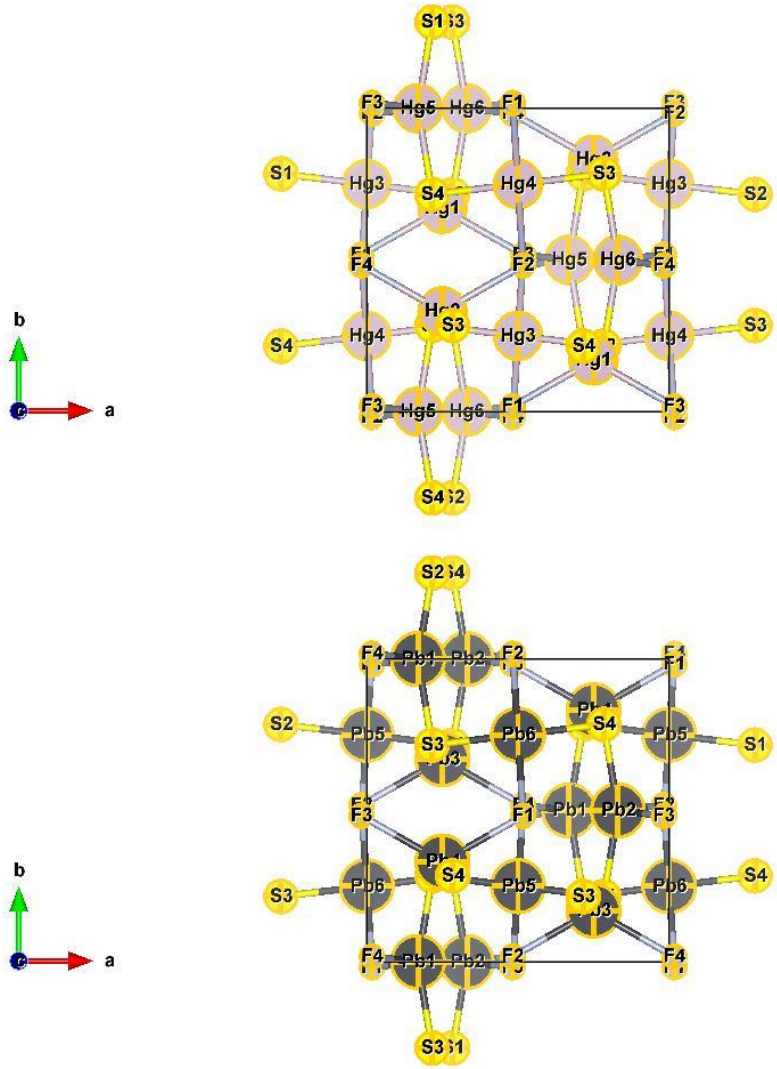

Fig. 3(a) and 3(b): Unit cell structure for both the compounds having a cubic structure. The Hg and Pb resides at corners, sulfur at the center and fluorine atoms are preferably on the faces respectively of single cubic unit cell.

3.2 Optical properties

The information about the complex dielectric function is related to the corresponding energy band structure of solid materials. The well known optical spectroscopy analysis is a dominant mean to determine the overall band behavior of solids [24,25]. Therefore we used the precise FPLAPW calculations to figure out the optical spectra.

Fig. 4(a) and 4(b) shows spectrum of the real and imaginary parts of the complex dielectric function versus photon energy for the two materials. The interpretation in terms of electronic structure for this spectrum is presented in the Fig. 1 of the band gapes of these materials, which clarify the manner that both the compounds absorb the incident radiations. Knowing the imaginary part of the complex dielectric function and using Kramers–Kronig relations we calculated its real part and various optical constants are then computed which describe the propagation of the electromagnetic wave throughout the materials [22]. In the existence of an external electromagnetic field the linear response of a system is usually described by the frequency dependent dielectric function $\varepsilon(\omega) = \varepsilon_1(\omega)+i\varepsilon_2(\omega)$, which are in association with the electronic structure of the materials, here $\varepsilon_1(\omega)$ and $\varepsilon_2(\omega)$ are the real (dispersive) and the imaginary (absorptive) parts of the complex dielectric function. The structures which appear in the spectra of $\varepsilon(\omega)$ primarily describe the transitions of electrons, that might be either inter band or intra band. In semiconductors, absence of intra band transitions, structures in $\varepsilon(\omega)$ are caused by the transitions of electrons between the occupied states in V.B and the unoccupied states in C.B along high symmetry points in the BZ. In addition to this a single peak in $\varepsilon_2(\omega)$ possibly will not correspond to a single transition because there may occur too many transitions simultaneously at energy which corresponds to a single peak. The momentum matrix elements is used to evaluate $\varepsilon_2(\omega)$ and the real part of the dielectric function can be derived from $\varepsilon_2(\omega)$. We took two non zero (xx = yy and zz) components of dielectric tensor $\varepsilon(\omega)$. The (xx=yy) component corresponds to the electric field which is perpendicular and the parallel (zz) to corresponding c-axis. We labeled these components as $\varepsilon^{xx}(\omega) = \varepsilon^{yy}(\omega)$ *and* $\varepsilon^{zz}(\omega)$. The average of these components i.e. $\varepsilon^{average}(\omega) = \varepsilon^{xx}(\omega) + \varepsilon^{yy}(\omega) + \varepsilon^{zz}(\omega)$ /3 is taken. The other energy dependent optical parameters are determined by using the obtained values of $\varepsilon_1(\omega)$and $\varepsilon_2(\omega)$. The evaluated optical parameters of the two materials in the present work with modified Becke–Johnson (mBJ) shows significant anisotropy at lower energy which is due to difference in the energy band gap. The critical point (i.e. absorption edge) for $Hg_3(SF)_2$, and $Pb_3(SF)_2$ lay at nearly 1.5 eV and 0.3 eV respectively. It is also clear from the fig 4(b) that a major peak in imaginary part of the spectra i.e $\varepsilon_2(\omega)$ arises at 3.99 eV and 8.41 eV for $Hg_3(SF)_2$ and $Pb_3(SF)_2$ respectively. The corresponding overall spectra at higher energy confirm almost similar behavior for the two compounds and are in a close agreement with the calculated band gap figures. The imaginary spectra $\varepsilon_2(\omega)$ shows that the two peaks are at energy > 0.5 eV for $Hg_3(SF)_2$ and showing higher peak which is at energy > 6 eV. The peaks in the imaginary part $\varepsilon_2(\omega)$ are because of the electric dipole transitions in-between the occupied and the unoccupied states. We used our calculated density of states of the two materials and relate them to the optical spectra to

investigate the origin of the peaks in the optical spectra. The signals which corresponds to transitions between the VBM and CBM in $\varepsilon_2(\omega)$ can be explained on the basis of our calculated electronic structure, the spectral peaks generally originated due to transitions from S-p and F-p states of the valence band to Hg-*d* state of the conduction band. When the absorption start, the peak rise rapidly for $Hg_3(SF)_2$ and became stronger than that for $Pb_3(SF)_2$. Then, beyond 8.0 eV, the two compounds showed almost the similar behavior, where at higher value of energies, $\varepsilon_2(\omega)$ decays rapidly at the same rate. The absorption coefficient $I(\omega)$ as an important factor gives information related to decay of light intensity per unit distance in a medium. The frequency dependent absorption coefficients for the two materials are shown in Fig.5(a) which shows that the change in frequency is described in terms of energy which ranges from 0 to 14 eV. The figure illustrate sharp edge of absorption coefficient which exists near 1 eV and 2.7 eV for $Hg_3(SF)_2$ and $Pb_3(SF)_2$ respectively. It has also been observed that there is no absorption for photon energy less than 2.6 ev and 0.9 e V for $Hg_3(SF)_2$ and $Pb_3(SF)_2$ respectively. However with greater photon energy than the corresponding values, the absorption coefficient increases, which might be associated with the indirect band gap values for the two materials. Many peaks are observed within the studied energy range, whose structure can be understood from inter band transitions between the valence band and conduction band. Materials having wide band gap acquire the property of having sharp edges present in spectrum of absorption coefficients which allows only suitable energy photons to enter into the material to excites electrons form VB occupied levels to the CB unoccupied levels. This property confirm that these materials can be recommend as prospective candidates for their diverse applications in optoelectronic devices working in the ultraviolet frequency range. The calculated energy loss function $L(\omega)$ is a significant parameter which illustrate the energy loss for electrons moving in a material. The peaks in energy loss function $L(\omega)$ shown in Fig.5(a) gives us brief details about characteristics related to plasma resonance and associated frequency called plasma frequency. There is no energy loss for photons having energy less than 2.4 eV and 0.9 eV for $Hg_3(SF)_2$ and $Pb_3(SF)_2$ respectively, but when the photons exceed these value of energy, the energy loss will start increasing and get the maximum peak at 12.1 eV and 11.02 eV for $Hg_3(SF)_2$ and $Pb_3(SF)_2$ respectively. The observed peaks in the energy loss function are mainly associated with the plasma frequency and are treated as an interface between metallic and dielectric behavior. In order to investigate the surface behavior of the these materials, we measured its reflectivity $R(\omega)$ which is the ratio of incident power to reflected power. Fig. 5(b) represents reflectivity versus energy for the two materials which shows that the zero frequency limit of reflectivity is equal to 0.129 and 0.247 for $Hg_3(SF)_2$ and $Pb_3(SF)_2$ respectively. It then increases from its zero limit and reached at the highest peak of reflectivity at 4.424 eV and 7.83 eV for $Hg_3(SF)_2$ and $Pb_3(SF)_2$ respectively. These peaks results due to inter band transition between valence band and conduction band. On the other hand, the minimum reflectivity value occurs as a result of cooperative effect of plasma resonance. The Imaginary part of dielectric function is used to measure the depth investigation of plasma resonance [25]. Fig. 5(c) and 5(d) shows the broad spectrum of refractive index and extinction coefficient respectively over wide range of energy.

Which illustrate that the spectrum of $n(\omega)$ nearly follow $\varepsilon_1(\omega)$ pattern. Two materials maintain their positive value of refractive index which shows that they are not a negative index metamaterials. In the middle region of the graph, we observe various humps which disappear at a higher value of photon energy. It is due to the fact that the material starts absorbing high energy photons and will no longer remain transparent beyond certain value of energy. At this value of energy, the refractive index becomes less than unity which can be easily seen from Fig. 5(c). Value of refractive index with less than unity express that group velocity ($v_g=c/n$) of the falling radiation becomes greater than speed of light. This shows that group velocity will move toward the negative domain and the nature of the medium will not remain linear. In other words, this reveals that the material will convert to superluminal medium for high energy photons [26-27]. The extinction coefficient is deduced from the complex dielectric function, the response of $k(\omega)$ is closely related with the response of $\varepsilon_2(\omega)$[28]. The extinction coefficient shown in the Fig. 5(e) gives information related to the absorption of light and absorption characteristics at the band edges. It also defines all the linear optical properties. The peaks in the extinction coefficient $k(\omega)$ are due to the inter band transition of electrons from valence band to conduction band. The greater magnitudes of the curve in the extinction coefficient $k(\omega)$ are noticed for photon energies in the range from 2 eV to 10 eV. To the best of our knowledge, there is lack of data available on the electronic and optical properties of $Hg_3(SF)_2$ and $Pb_3(SF)_2$. We therefore hope that this work will motivate researchers to do experimental studies along with theoretical studies using different exchange-correlation functional, so we can compare our results with them to get better understanding about these materials.

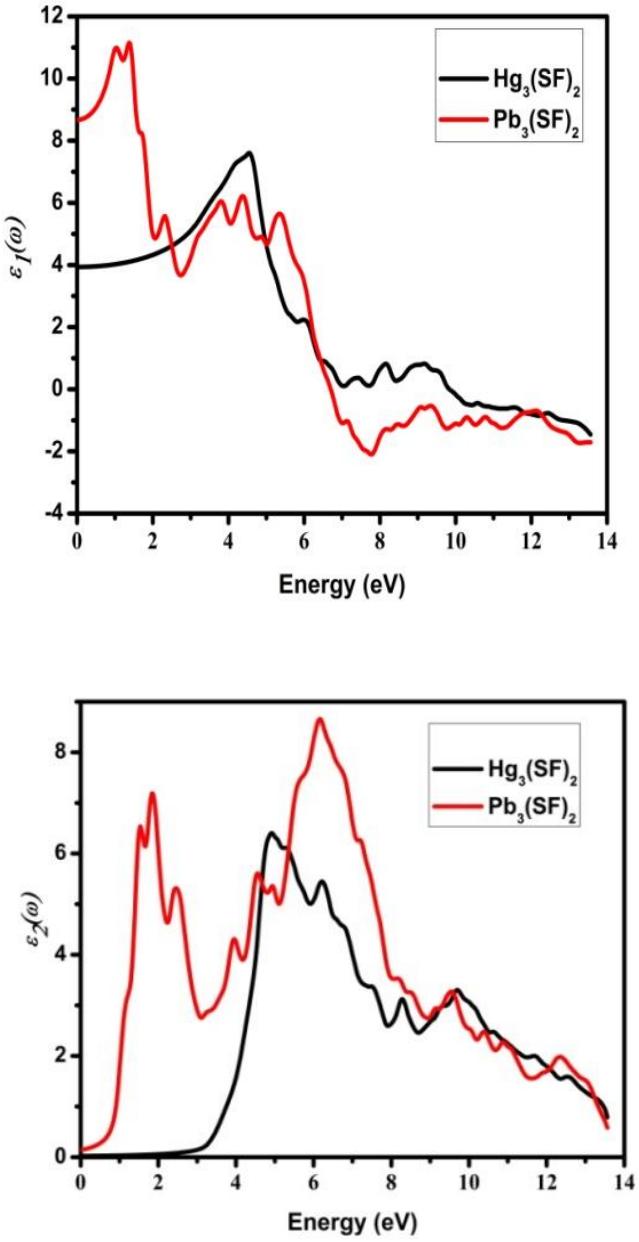

Fig. 4(a) and 4(b): Frequency dependent real and imaginary parts (ε_1 *(ω)* and $i\varepsilon_2$ *(ω)*) of dielectric functions of cubic phase of $A_3(SF)_2$ where A= (Hg, Pb)

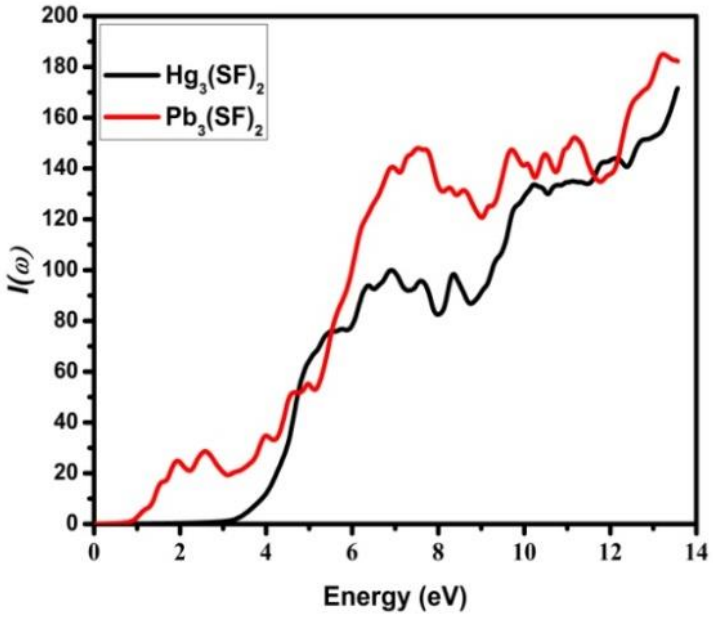

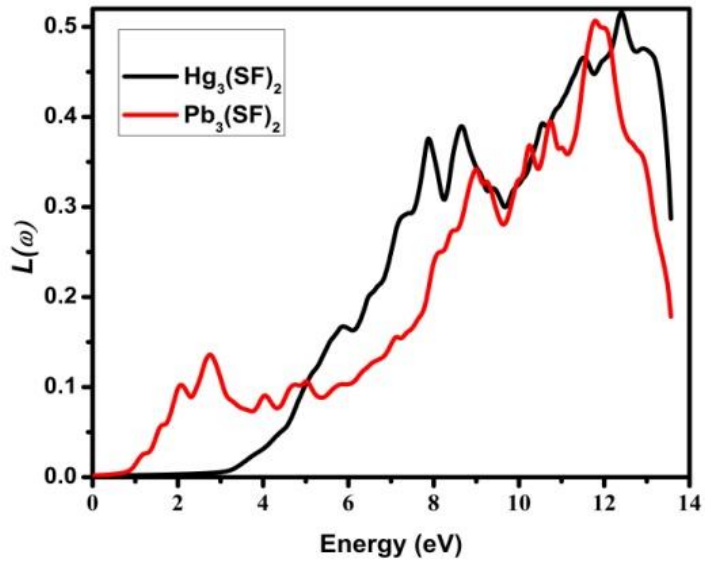

Fig. 5(a) and 5(b): Frequency dependent Absorption coefficient *I(ω)* and energy loss function *L(ω)* of cubic phase $A_3(SF)_2$ where A= (Hg, Pb)

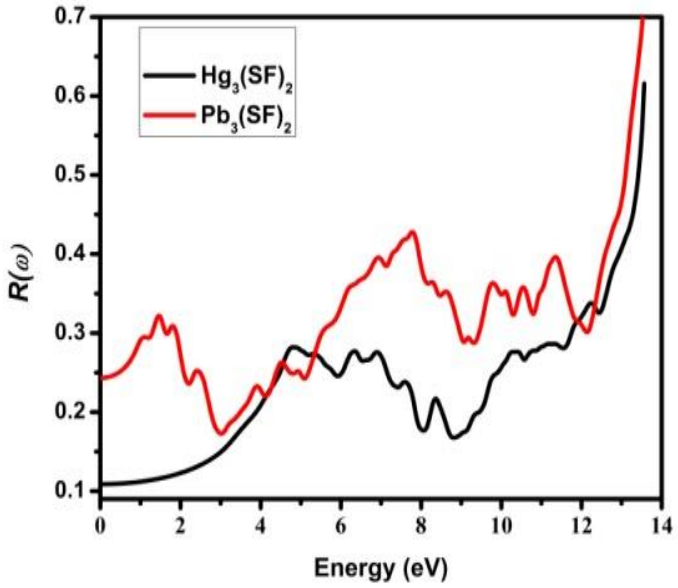
0.7
0.6
0.5
0.4
0.3
0.2
0.1
R(ω)
Hg3(SF)2
Pb3(SF)2
0
2
4
6
8
10
12
14
Energy (eV)

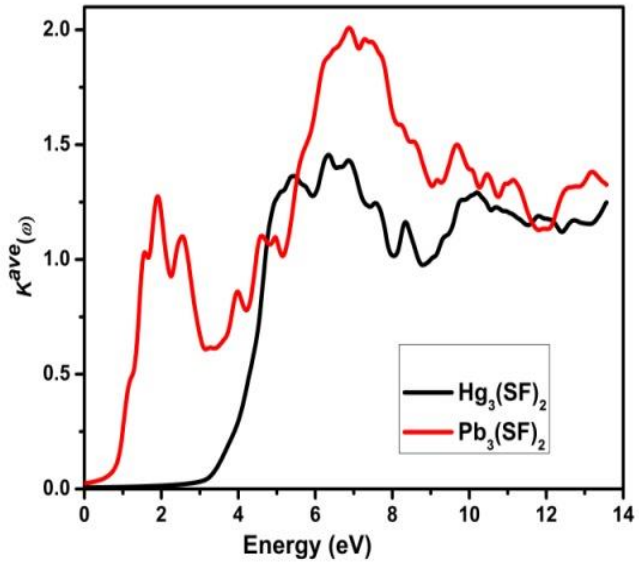

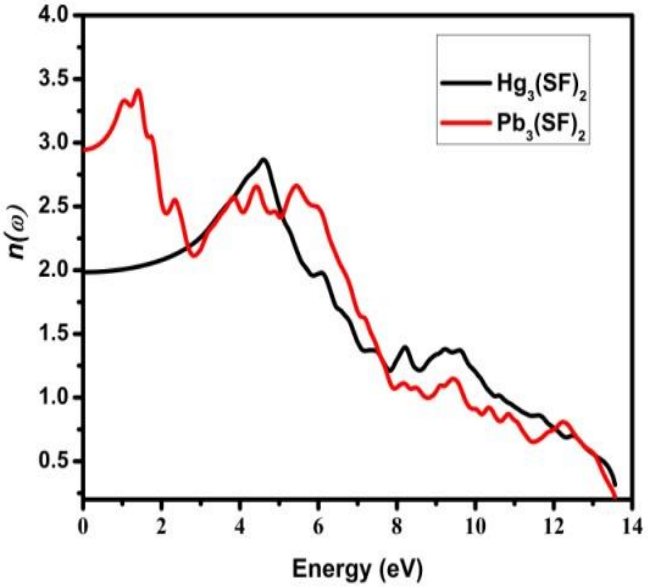

Fig. 5(c), 5(d), 5(e): Frequency dependent Reflectivity *R(ω)*, Refractive index *n(ω)* and Extinction coefficient *k(ω)* for the $A_3(SF)_2$ where A= (Hg, Pb)

4. Conclusion

In summary the structural, electronic optical properties of cubic phase $A_3(SF)_2$ A= (Hg, Pb) are calculated using the well known modified Becke–Johnson (mBJ) method within the framework of density functional theory. The electronic band structure of cubic phase $A_3(SF)_2$ demonstrate that the material is found to be an indirect band gap material. These calculated band gaps values are used to investigate band gap bowing parameter, which reveals that the materials deviates principally from the linear combination. The partial densities of states indicate there is major hybridization between the electronic states of the elements of these two materials. The complex dielectric function and various optical constants are computed using Kramers–Kronig relations. These optical parameters show that there is significant anisotropy at lower energy which is due to difference in the energy band gap. The peaks in the real and imaginary part $\varepsilon(\omega)$ are mostly because of the electric dipole transitions in-between the occupied and the unoccupied states. There are sharp edges present in spectrum of absorption coefficients which allows only suitable energy photons to enter into the material to excites electrons form VB occupied levels to the CB unoccupied levels. This property confirm that these materials can be recommend as prospective candidates for their diverse applications in optoelectronic devices working in the ultraviolet frequency range The observed peaks in the energy loss function are mainly associated with the plasma frequency and which is treated as an interface between metallic and dielectric behavior. These two materials maintain their positive value of refractive index which shows that they are not a negative index metamaterials. As there is lack of data available on the electronic and optical properties of cubic phase $Hg_3(SF)_2$ and $Pb_3(SF)_2$ so we hope that this work will motivate researchers to do experimental studies along with theoretical studies using different exchange-correlation functional.

References

[1] T. Yajima, H. Suzuki, T. Yogo, H. Iwahara, Protonic conduction in SrZrO3-based oxides, Solid State Ionics 51 (1992) 101-107.

[2] H. Iwahara, T. Yajima, T. Hibino, H. Ushida, Performance of solid oxide fuel cell using proton and oxide ion mixed conductors based on BaCe1 x Sm x O3 a, J. Electrochem. Soc. 140 (1993) 1687-1691

[3] N. Choundhury and B. K. Sharma, Thin Solid Films. 519 (2011) 2132

[4] G. D. Mahan, Solid State Phys. 51, (1998) 81.

[5] K.-F. Hsu, S. Loo, F. Guo, W. Chen, J. S. Dyck, C. Uher, T. Hogan, E. K. Polychroniadis, and M. G. Kanatzidis, Science 303, (2004) 818

[6] R. A. Hein and E. M. Swiggard, Phys. Rev. Lett. 24, (1970) 53

[7] S.K. Mehta, S. Kumar, S. Chaudharya, K.K. Bhasina, Nanoscale 2, (2010)145

[8] N. Srinivasan, S. Thirumaran, S. Ciattinib, RSC Adv. 4, (2014) 22971

[9] X. Liu, R. Liu, Y. Tang, L. Zhang, X. Houab, Y. Lv, Analyst 137, (2012) 1473

[10] E. ASHMOLE. Theatrurn Chemicum Brittanicum. - London. 1652. p. 125-127.

[11] Matthias Wei Z. Naturforsch., 69b, (2014) 665–673

[12] G. M. Sheldrick, Acta Crystallogr., A64, (2008) 112– 122.

[13] J-P. Zou, G-C. Guo, S-P. Guo,a Y-B. Lu, K-J Wu, M-S Wanga and J-S Huanga j. Dalton Trans., (2007) 4854–485

[14] A.C. Wibowo, C.D. Malliakas, D.Y. Chung, J. Im, A.J. Freeman, and M. G. Kanatzidis, Mercury Bismuth Chalcohalides, Hg3Q2Bi2Cl8 (Q = S, Se, Te): Syntheses, Crystal Structures, Band Structures, and Optical Properties, Inorg. Chem 52, (2013).

[15] Z. Feng, H. Hu, S. Cui, C. Bai, First-principles study of optical properties of SrZrO3 in cubic phase, Solid state Commun. 148 (2008) 472-475.

[16] P. Hohenberg, W. Kohn, Inhomogeneous electron gas, Phys. Rev. 136 (1964) B864.

[17] W. Kohn, L.J. Sham, Self-consistent equations including exchange and correlation effects, Phys. Rev. 140 (1965) A1133.

[18] K. Schwarz, P. Blaha, G. Madsen, Electronic structure calculations of solids using the WIEN2k package for material sciences, Comput. Phys. Commun. 147 (2002) 71-76.

[19] I. Levin, et al., Phase equilibria, crystal structures, and dielectric anomaly in the BaZrO3eCaZrO3 system, J. Solid State Chem. 175 (2003) 170-181

[20] F. Tran and P. Blaha, Phys. Rev. Lett. 102, (2009) 226401

[21] S. Cottenier, Density Functional Theory and the Family of (L) APW-methods: a Step-by-step Introduction, vol. 4, Instituut voor Kern-en Stralingsfysica, KU Leuven, Belgium, (2002) p. 41

[22] V.V. Atuchin, B.G. Bazarov, T.A. Gavrilova, V.G. Grossman, M.S. Molokeev, Z.G. Bazarova, J. Alloys Compd. 515 (2012) 119

[23] Ali Z, Khan I, Ahmad I, Khan M S and Asadabadi S J Mat. Chem. Phys. 162 (2015) 308-315

[24] B. Amin, R. Khenata, A. Bouhemadou, I. Ahmad, M. Maqbool. Physica B 407, (2012) 2588–2592

[25] D.R. Penn, Wave-number-dependent dielectric function of semiconductors, Phys. Rev. 128 (1962) 2093.

[26] A.M. Fox, Optical Properties of Solids, vol. 3, Oxford university press, (2001).

[27] L.J. Wang, A. Kuzmich, A. Dogariu, Gain-assisted superluminal light propagation, Nature 406 (2000) 277-279.

[28] M. Fox, Optical Properties of Solids, 2nd ed., Oxford University Press, Oxford (2010).